Radiative heat load distribution on the EU-DEMO first wall due to mitigated disruptions

Nuclear Materials and Energy 25 (2020) 100824

Contents lists available at ScienceDirect

Nuclear Materials and Energy

journal homepage: www.elsevier.com/locate/nme

# Radiative heat load distribution on the EU-DEMO first wall due to mitigated disruptions

M. Moscheni [a,*], M. Carr [b], S. Dulla [c], F. Maviglia [c], A. Meakins [b], G.F. Nallo [a], F. Subba [a], R. Zanino [a]

[a] NEMO Group, Dipartimento Energia, Politecnico di Torino, Corso Duca degli Abruzzi 24, 10129 Torino, Italy
[b] Luffy AI, Culham Science Centre, Abingdon OX14 3DB, United Kingdom
[c] EUROFusion PMU, Boltzmannstrasse 2, Garching bei Munchen, Germany

ARTICLE INFO

*Keywords:*
Nuclear fusion
EU-DEMO
Disruption mitigation
Monte Carlo
Radiative load
First wall

ABSTRACT

The EU-DEMO First Wall (FW) will be a relatively thin structure. In order not to damage this layer, heat loads distributed onto the wall should be carefully controlled. In the case of transient events, as for example plasma disruptions, the steady-state heat load limit ($\sim 1-2$ MW/m$^2$) can be largely exceeded for a timespan sufficiently long to cause damages. Therefore, when the control system detects an upcoming disruption, Shattered Pellet Injection (SPI) or Massive Gas Injection (MGI) mitigation techniques can be employed to inject impurities and switch off the plasma safely. In the present work, the Monte-Carlo ray-tracing code CHERAB is used to compute the radiative heat load distribution on the EU-DEMO Plasma Facing Components (PFCs) due to a mitigated plasma disruption. By applying *ad-hoc* techniques to improve the quality of the Monte Carlo calculation, we obtain a peak radiative load of $\sim 490$ MW/m$^2$ on the PFCs, which is $\sim 25\%$ lower than previous estimates.

## 1. Introduction

The EU-DEMO FW will be a relatively thin structure (mainly due to Tritium-breeding requirements), with a 2–3 mm layer of structural material (Eurofer) and a W coating [1,2]. To compensate for differences in the coefficients of thermal expansion, a functionally graded interlayer is interposed between Eurofer and W [3], resulting in a coating thickness of 2 mm. To prevent damaging the W layer, heat loads distributed onto the FW should be carefully controlled. In steady-state nominal operation, the maximum acceptable load is $\sim 1-2$ MW/m$^2$ [4]. In the case of transient events, e.g. the thermal quench of a plasma disruption, this limit can be largely exceeded. Considering the worst possible EU-DEMO scenario of a non-mitigated thermal quench, it is suggested that ablation of W would be surely reached if no mitigation strategy is implemented [5]. Therefore, when the control system detects an upcoming disruption, impurities (in the form of shattered pellets or massive amounts of gas) can be injected in the plasma to mitigate the event [6]. This mitigation aims at enhancing as much as possible the radiation emission to spread the plasma internal energy onto the entire FW surface so reducing the localized peaks.

In order to precisely assess the radiative load distribution onto the EU-DEMO FW during the thermal quench of a mitigated disruption, we run the Monte Carlo (MC) ray-tracing code CHERAB [7–9]. As CHERAB is capable of handling sophisticated 3D wall geometries, we can take into account the details of the latest design of the EU-DEMO FW. We use a radiation source distributed along the vertically-displaced last closed flux surface (VD-LCFS), to mimic the emission distribution during the mitigated disruption. This choice allows to benchmark our result against previous estimates [10].

In this work, we also present a procedure to improve the Monte Carlo statistics in the CHERAB code [11], reducing the noise for a given number of MC samples (rays). By applying our improved technique, the estimated peak power load on the outboard upper limiter is shown to be of $\sim 490$ MW/m$^2$, i.e. 25% lower than previous estimates [10].

The paper is organized as follows: in Sec. 2, we describe the methodology, consisting of the simulation setup and of the techniques to improve precision and accuracy; in Sec. 3, the results are discussed, also in comparison with the previous ones; in Sec. 4, we present conclusions and perspective of this work.

* Corresponding author.
*E-mail address:* matteo.moscheni@polito.it (M. Moscheni).

https://doi.org/10.1016/j.nme.2020.100824
Received 31 July 2020; Received in revised form 7 October 2020; Accepted 26 October 2020
Available online 1 November 2020

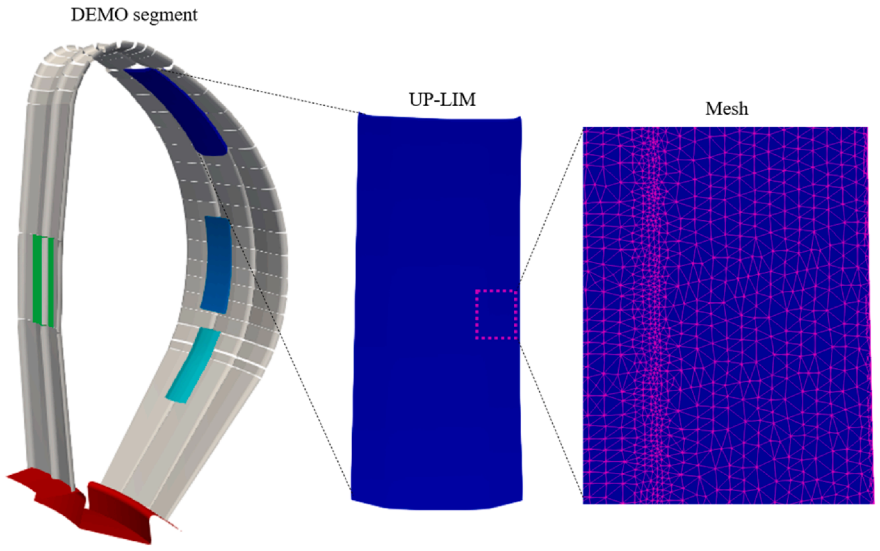


| PFC | DIV | BB-FW | IN-LIM | UP-LIM | EQ-LIM | LOW-LIM |
|---|---|---|---|---|---|---|
| Periodicity | 22.5° | 22.5° | 90° | 45° | 90° | 90° |

**Fig. 1.** Geometry of the simulated EU-DEMO sector, provided with four limiters: inner (IN-LIM), upper (UP-LIM), equatorial (EQ-LIM) and lower (LOW-LIM). The zoom on UP-LIM shows the unstructured triangulation defined on its perfectly absorbing surface.

## 2. Methodology

### 2.1. Simulation setup

#### 2.1.1. Input: Computational mesh

The CHERAB code is based on the ray-tracing engine Raysect [12,13]. The processes encountered in the propagation of light from the source ($[\mathrm{W/m^3/sr}]$) to the target surface (computational mesh) are approximated via MC integration. In the present work, the EU-DEMO FW is subdivided into 89 sub-pieces according to the latest CAD files provided by EUROfusion [14]. On each sub-piece, an unstructured, non-uniform triangulation is defined with a suitable localized refinement (see Fig. 1) to guarantee a satisfactory resolution of the gradients of the radiative load distribution (average linear size of the triangles $\lesssim 1$ cm). This triangulation represents the computational mesh of the simulation.

In CHERAB, each triangle becomes a radiation detector. A number $N_{\mathrm{ray}}$ of rays are shot from each detector[1]. By tracing the intersections of the rays with radiation sources, the radiation heat load $q_i\ [W/m^2]$ over each detector is computed, alongside with the corresponding statistical error $\Delta q_i\ [W/m^2]$. By combining the heat load measurements, the total power $P_{\mathrm{tot}}$ [W] reaching the surface and its absolute error $\Delta P_{\mathrm{tot}}$ [W] [15] can be evaluated and compared with the expected output $P^*_{\mathrm{tot}}$. An agreement in this respect is a necessary, though not sufficient, condition to conclude that the radiative heat load distribution is reliable [11].

Despite the periodicities of the PFCs along the toroidal direction suggesting that the irradiation should be simulated over 1/4 of the tokamak, we take into consideration 1/16 of the EU-DEMO chamber, choosing a sector equipped with all the limiters, i.e. the PFCs of most concern (see Fig. 1). This choice allows saving computational time. The tiny gaps left behind by the arrangement of the pieces (lack of water-tightness of the mesh) are to be taken into account in the energy conservation check.

The surface of the whole sector is assumed to be a perfect radiation absorber. No reflection is modelled at this stage because: (i) it is not foreseen to markedly influence the result; (ii) it requires additional pieces of information; (iii) it would introduce an important increase in the computational cost (which is already non negligible).

#### 2.1.2. Input: Radiation source

We employ a total power radiated $P^*_{\mathrm{tot}} = 500$ GW, consistently with [10]. The source is built by placing $\sim 100$ annular-like elements along the VD-LCFS [14] to approximate a continuous distribution[2] (see Fig. 2, right). Each element is characterized by a square poloidal cross section with side length $l = 1$cm, axisymmetrically mapped along the toroidal direction $\varphi$ (Fig. 2, left). The assumed toroidal symmetry of the source is consistent with the similarity between the characteristic toroidal revolution time and the duration of the thermal quench [11]. The power $P_V$ emitted per unit volume and unit steradian $[\mathrm{W/m^3/sr}]$ is the same for all the annular sources.

No space, nor wavelength, nor time dependence is considered: $P^*_{\mathrm{tot}}$ is assumed to be constantly radiated during the whole thermal quench (conservatively lasting $\tau_{\mathrm{TQ}} = 1$ ms) [16–18] giving a constant $P_V$ in time.

All these features match the ones of the previous work [10].

### 2.2. MC statistics: Improvement of simulation quality

#### 2.2.1. PDF and peak power load analysis

We now consider the mesh defined over a single sub-piece (out of the total 89). With $q$ standing for a generic heat load, the Probability Density Function (PDF) $f(q)$ of the collection of measurements $\{q_i\}$ over the mesh is such that $f(q)dq$ represents the probability of finding a detected heat load $q_i$ in the interval $[q; q+dq]$ [19]. Whatever the actual overall PDF $f(q)$, each $q_i$ is one realization of an unknown normally distributed

[1] Actually, the radiative load acquisition performed by each detector follows a more involved (rendering) procedure [11]. Each detector usually ends up shooting an integer multiple of $N_{\mathrm{ray}}$. Nonetheless, there is no difference in practice.

[2] In principle, CHERAB allows to build a continuous power emission distribution. However, this approach is more computationally efficient.

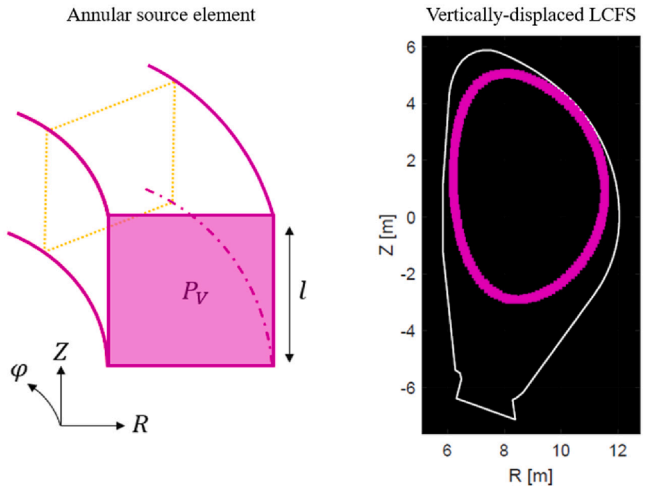


**Fig. 2.** Left: representation of one annular emitter, the fundamental brick of the radiation source geometry. Right: VD-LCFS in the poloidal plane. The white contour is a schematic representation of the 2D projection of the 3D structure of Fig. 1. The square cross sections of the emitters are enlarged for the sake of a better visualization.

random variable whose broadening (standard deviation $\sigma$) is approximately quantified by the corresponding error $\Delta q_i$. In other words, if the measurement of the $i^{\text{th}}$ detector only is repeated $N \gg 1$ times, a Gaussian distribution would be recovered. Although this is never done in practice, the practically relevant circumstance of a uniform irradiation over $N$ identical detectors must give the same result: instead of "the measurement of one detector is repeated $N \gg 1$ times" it is "one measurement is carried out by $N \gg 1$ equivalent detectors". According to Fig. 3 (test case with $N = 5000$), a Gaussian distribution of $\{q_i\}$ is recovered ($R^2 > 0.95$), as expected. Therefore, a uniform irradiation leads to a Gaussian PDF due to the non-zero error. It follows that, with a lower and lower probability (depending on $N$), a generic $q_i$ may lie farther and farther away from the average (hopefully exact, though unknown in practice) value $\mu$. As a consequence, a generic $q_i$ could be affected by an error significantly greater than the $\Delta q_i$ computed by the code. In the present work, the error on the maximum detected radiative load $q_{\max}$ can be proved to be as large as $\sim +4\Delta q_i$ ($+4\sigma$) [11] (see Fig. 3). The exact maximum radiative load $q_{\max}^{\text{exact}}$ then lies in the interval $(q_{\max} - 4\sigma; q_{\max})$ which represents a suitable, not necessarily thin, error bar.

Considering the more general case of non-uniform irradiation, $f(q)$ can be of arbitrary shape due to the presence of gradients in the heat load. However, according to [11]: (i) the above-mentioned discussion about the error over $q_{\max}$ holds in this circumstance as well; (ii) the resolution of gradients themselves cannot be guaranteed: if the statistical fluctuation is too high, the result would lack of precision, gradients would be completely lost, the radiative load would turn out to be uniform-like and Gaussian peaks would be recovered. Instead, a high-precision condition is set when sharp edges and/or asymmetries of the structures of $f(q)$ appear.

#### 2.2.2. Averaging procedure

It is common practice to reduce the statistical uncertainty $\Delta q_i$ of the outcome $q_i$ by increasing the number of MC samples, i.e. the number of rays $N_{\text{ray}}$ shot by the $i^{\text{th}}$ detector. Indeed, the relative error $\epsilon_i = \Delta q_i / q_i$ is such that $\epsilon_i \propto N_{\text{ray}}^{-1/2}$ [11]. However, the computational cost approximately[3] scales as $\propto N_{\text{ray}}$. Hence, merely enhancing $N_{\text{ray}}$ to get a more precise result may not be feasible in practice.

For this reason, we develop an averaging procedure (AVG) based on

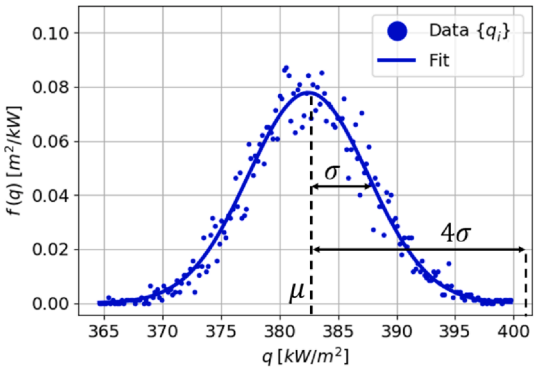


**Fig. 3.** Uniform irradiation in the test case with $N = 5000$ detectors gives a Gaussian-like PDF due to the non-zero error introduced by the MC integration. Measurements $\sim 4\sigma$ away from the exact, average value $\mu$ are found. Blue points are a representative subset of $\{q_i\}$. (For interpretation of the references to colour in this figure legend, the reader is referred to the web version of this article.)

the idea of smoothing out the statistical fluctuation by suitably working on the set $\{q_i\}$. To this purpose, consider one detector (i.e. mesh triangle) $\mathfrak{D}_i$ which has acquired $q_i$ and a number $(N_i - 1)$ of adjacent detectors, i.e. sharing with $\mathfrak{D}_i$ at least one vertex (see Fig. 4). Let the index $k$ run over the collection of such $N_i$ detectors, $\mathfrak{D}_i$ included. The averaged radiative heat load $\langle q_i \rangle$ to be substituted to $q_i$ can be written as the weighted average:

$$\langle q_i \rangle = \frac{\sum_{k=1}^{N_i} A_k q_k}{\sum_{k=1}^{N_i} A_k} \tag{1}$$

The procedure is then repeated for all detectors in the mesh. This yields the overall averaged heat load profile. This approach shows some relevant features [11]: (i) averaging over adjacent triangles mainly smooths out the statistical fluctuation (which appear on this very spatial scale) while satisfactorily (though not perfectly) maintaining the macroscopic gradients implied by the irradiation (which occur over a larger spatial scale). "Not perfectly" means that an error associated to AVG is introduced, which can however be safely monitored; (ii) to be consistent with the physics of radiation transport, the average must be performed only on the neighboring triangles which do belong to the "same surface", as shown in Fig. 4. This is practically ensured by suitably checking the orientation of the normals; (iii) the error $\Delta\langle q_i \rangle$ over $\langle q_i \rangle$ follows from $\{q_k\}$ and the errors $\{\Delta q_k\}$, according to [15]. Hence, the computation of $\langle q_i \rangle$ (Eq. (1)) and $\Delta\langle q_i \rangle$ does not depend on $N_{\text{ray}}$, but rather on $N_i$ (almost constant throughout the mesh). In conclusion, the fundamental MC law still holds for the averaged quantities, i.e. $\Delta\langle q_i \rangle / \langle q_i \rangle \propto N_{ray}^{-1/2}$, and convergence studies can be carried out even after the application of AVG; (iv) AVG cannot entirely substitute enhancing the number of rays but it can be a cheap auxiliary post-processing tool to improve precision.

## 3. Results and discussion

### 3.1. Benchmark against previous work

The most relevant input parameters of the simulations are listed in Table 1. The source geometry and the number of rays of the updated simulation "$N_{\text{ray}} = 250$ – AVG = no" are chosen to match the ones of "[10] – $N_{\text{ray}} = 250$ – AVG = no" to have a well-posed benchmark. The only (minor) difference between the two cases is the design of the PFCs.

First of all, the energy conservation is accurately satisfied and the missing power in "$N_{\text{ray}} = 250$ – AVG = no" ($-3\%$) can be carefully

[3] Additional parameters are involved in the power load computation [11].

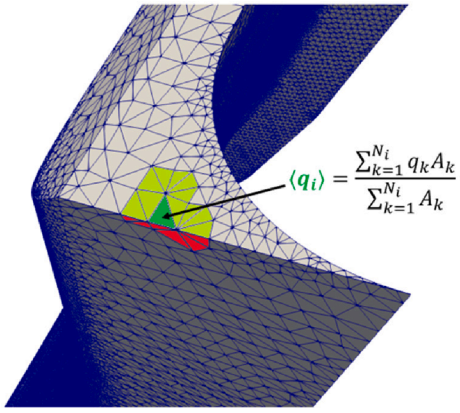


**Fig. 4.** Top part of the mesh defined over UP-LIM and schematic of the averaging procedure. Among the triangles sharing at least one vertex with the reference one (dark green), only the light green ones are to be considered in the computation of the average power load $\langle q_i \rangle$ (Eq. (1)). The red ones are excluded (see text). (For interpretation of the references to colour in this figure legend, the reader is referred to the web version of this article.)

**Table 1**
Main settings and outcomes of the different simulations with VD-LCFS radiation source. The number of significant digits of each output quantity follows from its precision. The case "$N_{ray} = 10000$ – AVG = yes" was run for UP-LIM only. All simulations have been run with OMP parallelization on a 16x2 cores cluster node with Intel® Xeon® Gold Scalable Processor Gold CPU 6130 @2.10 GHz.

| Work | $N_{ray}[-]$ | AVG | $\epsilon[-]$ | $q_{max}[MW/m^2]$ | $P_{tot}[GW]$ | CPU time [h] |
|---|---|---|---|---|---|---|
| [10] | 250 | no | 11.4% | $6.6{\cdot}10^2$ | 497.99/500 | – |
| (new) | 250 | no | 9.8% | $6.2{\cdot}10^2$ | 484.69/500 | 36 |
| | 2500 | yes | 1.2% | 488 | 484.352/500 | 72 + 1 |
| | 10000 | yes | 0.35% | 483 | – | – |

1 h is the computational cost of the AVG procedure for that case.

motivated in terms of lack of watertightness of the mesh[4] (see Sec. 2.1.1). Still, this missing power does not affect anyhow the computed radiative load distribution and, hence, it does not pose any threat to the reliability of the outcome.

Then, to perform a quantitative comparison we exploit the PDF of the measurements of "$N_{ray} = 250$ – AVG = no" and "[10] – $N_{ray} = 250$ – AVG = no" over UP-LIM (see Fig. 5), a representative PFC for such an analysis [11]. Their overlap is satisfactory, thus confirming the quantitative agreement between the two cases. The small discrepancies can be explained in terms of the small geometrical differences in UP-LIM.

As it is apparent from Fig. 5 in the light of Sec. 2.2.1, the precision of the calculation requires an improvement.

### 3.2. Simulations with increased number of rays and AVG

An improved simulation with $N_{ray} = 2500$ is run and AVG is carried out. The comparison against "$N_{ray} = 250$ – AVG = no" is pictured in Fig. 6.

It is clear that the unphysical statistical fluctuations, mostly observed in "[10] – $N_{ray} = 250$ – AVG = no", are substantially reduced. Furthermore, this allows for a more precise evaluation of the peak radiative load in both value and location. Indeed, in [10], $q_{max}$ had been significantly overestimated ( + 35%) and incorrectly located (elsewhere than on UP-LIM).

[4] Further subtle effects are involved but they can be shown to give a negligible contribution [11].

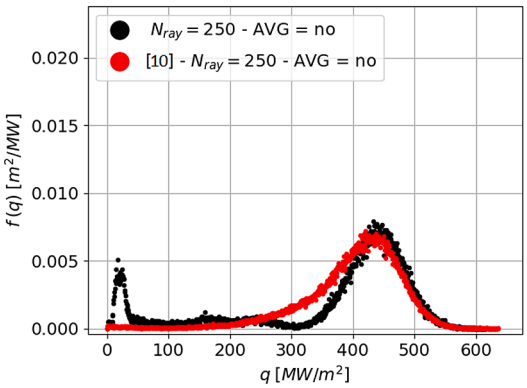


**Fig. 5.** The overlap of the PDFs over UP-LIM confirms a quantitative agreement of the current result with [10] in the case $N_{ray} = 250$. The lack of a perfect overlap is due to the different UP-LIM design and it is then of little relevance. Still, Gaussian-like peaks are symptoms of low precision (see Sec. 2.2.1).

Finally, we assess the convergence in terms of the number of rays by running the "reference" calculation "$N_{ray} = 10000$ – AVG = yes". We not only check the convergence on $q_{max}$, but we also verify that its associated PDF on UP-LIM, where the peak heat load occurs, is practically superimposed to the PDF "$N_{ray} = 2500$ – AVG = yes" (see Fig. 7), thus ensuring the quantitative convergence of the entire radiative load distribution. Therefore, according to Sec. 2.2.1, we can reliably conclude that $q_{max}^{exact}$ lies in the interval $(q_{max} - 4\sigma; q_{max}) = (476; 488)$ MW/m$^2$ for the configuration considered.

The peak heat impact factor, defined as $\left(q_{max}\cdot\sqrt{\tau}\right)$, is commonly used to assess whether or not the heat load $q_{max}$ $[W/m^2]$ applied for the timespan $\tau$[s] eventually results in melting of the solid surfaces. Since, in the present work, with $q_{max} = 488 MW/m^2$ and $\tau = \tau_{TQ} = 1$ ms, the corresponding peak heat impact factor (15.4 MJ·m$^{-2}$·s$^{-0.5}$) lies above the W threshold ($\sim$ 10 MJ·m$^{-2}$·s$^{-0.5}$ [14,20]), melting of the W layer is reached. However, further studies with more realistic sources are required to assess the actual risk of melting.

## 4. Conclusions and perspective

The CHERAB code is employed in this work to evaluate the radiative heat load distribution over the EU-DEMO PFCs due to a mitigated plasma disruption. The radiation source during this event is assumed to be toroidally symmetric and distributed along the vertically-displaced last closed flux surface.

After having verified the correct settings of the code by assessing the energy conservation and by comparing our results with those of an already existing simulation, two techniques for improving the simulation quality are proposed:

i. An averaging procedure that allows smoothing out the Monte Carlo statistical fluctuations of the computed heat load;
ii. A statistical analysis that allows testing the quality assurance of the result and providing a suitable error bar for the peak radiative load.

The converged CHERAB simulation gives a peak heat load $q_{max}$ of $\sim$ 490 MW/m$^2$ on the outboard upper limiter (UP-LIM, a sacrificial PFC), $\sim$ 25% lower than previous estimates [10], which also foresees the peak heat load to be incorrectly located elsewhere than on UP-LIM in [10].

A detailed computation of the radiative load distribution in the case of a full 3D radiation source, taking into account poloidal and toroidal asymmetries, could be performed with CHERAB but it is beyond the scope of the present work. However, a simplified way of taking into account asymmetries in the source is to scale up $q_{max}$ by a toroidal and poloidal peaking factor $\gamma$. By assuming $\gamma \sim 3$ as estimated for ITER

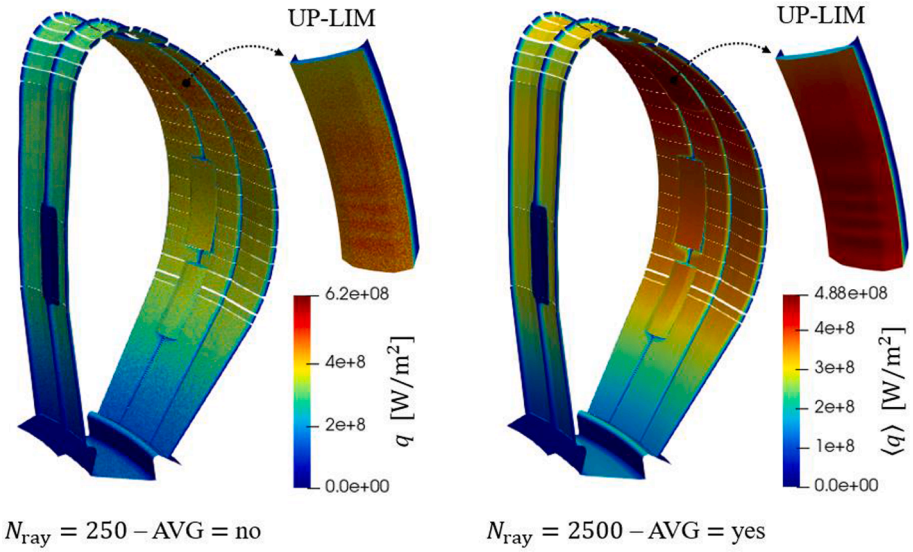


**Fig. 6.** The radiative heat load map ("$N_{ray} = 250 - AVG = no$") significantly improves after both the increase in $N_{ray}$ and the application of AVG ("$N_{ray} = 2500 - AVG = yes$"). In particular, $q_{max}$ is drastically reduced in the more precise simulation (right). Different scales are employed to emphasize these features.

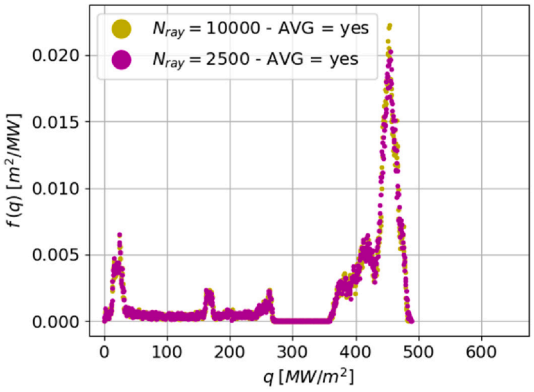


**Fig. 7.** The satisfactory overlap of the PDF computed with $N_{ray} = 10000$ and with $N_{ray} = 2500$ over UP-LIM suggests that, with $N_{ray} = 2500$, the output is already practically independent from the number of rays. These profiles are very different from those of Fig. 5, due to the enhanced precision (see Sec. 2.2.1).

[14,21], the resulting peak heat load is $\gamma \cdot q_{max} \sim 1500$ MW/m$^2$.

Nonetheless, even without applying any peaking factor, the corresponding peak heat impact factor turns out to be $\sim 15$ MJ$\cdot$m$^{-2}$s$^{-0.5}$, which is already above the W damage threshold of $\sim 10$ MJ$\cdot$m$^{-2}$s$^{-0.5}$ [14,20].

Since the radiation source was selected in a rough approximation to study the code convergence, further studies with more realistic sources are planned.

## CRediT authorship contribution statement

**M. Moscheni:** Methodology, Software, Validation, Formal analysis, Investigation, Data curation, Writing - original draft, Writing - review & editing, Visualization. **M. Carr:** Conceptualization, Methodology, Software, Supervision. **S. Dulla:** Formal analysis, Supervision. **F. Maviglia:** Conceptualization, Methodology, Writing - review & editing, Supervision, Project administration, Funding acquisition. **A. Meakins:** Conceptualization, Methodology, Software, Supervision. **G.F. Nallo:** Software, Formal analysis, Resources, Writing - original draft, Writing - review & editing, Visualization. **F. Subba:** Conceptualization, Formal analysis, Writing - original draft, Writing - review & editing, Supervision. **R. Zanino:** Conceptualization, Writing - review & editing, Supervision, Project administration, Funding acquisition.

## Declaration of Competing Interest

The authors declare that they have no known competing financial interests or personal relationships that could have appeared to influence the work reported in this paper.

## Acknowledgments

This work has been carried out within the framework of the EUROfusion consortium and has received funding from the Euratom research and training programme 2014-2018 and 2019-2020 under grant agreement No 633053. The views and opinions expressed herein do not necessarily reflect those of the European Commission.

Computational resources were provided by HPC@POLITO, a project of Academic Computing within the Department of Control and Computer Engineering at the Politecnico di Torino (http://www.hpc.polito.it).

## References

[1] F.A. Hernandez, P. Pereslavtsev, G. Zhou, H. Neuberger, J. Rey, Q. Kang, L. V. Boccaccini, E. Bubelis, I. Moscato, D. Dongiovanni, An enhanced, near-term HCPB design as driver blanket for the EU DEMO, Fusion Eng. Des. 146 (2019) 1186–1191.

[2] E. Martelli, A. Del Nevo, P. Arena, G. Bongiovì, G. Caruso, P.A. Di Maio, M. Eboli, G. Mariano, R. Marinari, F. Moro, R. Mozzillo, F. Giannetti, G. Di Gironimo, A. Tarallo, A. Tassone, R. Villari, Advancements in DEMO WCLL breeding blanket design and integration, Int. J. Energy Res. 42 (2018) 27–52.

[3] L. Forest, J. Aktaa, L.V. Boccaccini, T. Emmerich, B. Eugen-ghidersa, G. Fondant, A. Froio, A. Li, H. Namburi, H. Neuberger, J. Rey, L. Savoldi, D. Sornin, L. Vala, Status of the EU DEMO breeding blanket manufacturing R & D activities, Fusion Eng. Des. 152 (2020) 111420.

[4] F. Cismondi, Progress in EU Breeding Blanket design and integration, Fusion Eng. Des. 136 (2018) 782–792.

[5] R. Wenninger, R. Albanese, R. Ambrosino, F. Arbeiter, J. Aubert, C. Bachmann, L. Barbato, T. Barrett, M. Beckers, W. Biel, The DEMO wall challenge, Nucl. Fusion 57 (4) (9 Feb 2017).

[6] N. Commaux, D. Shiraki, L.R. Baylor, E.M. Hollmann, N.W. Eidietis, C.J. Lasnier, R. A. Moyer, T.C. Jernigan, S.J. Meitner, S.K. Combs, C.R. Foust, First demonstration of rapid shutdown using neon shattered pellet injection for thermal quench mitigation on DIII-D, Nucl. Fusion 56 (4) (2016) 46007.

[7] M. Carr, A. Meakins, cherab/core: Release v1.1.0, Zenodo, 2019.

[8] M. Carr, A. Meakins, A. Baciero, C. Giroud, CHERAB's documentation, 2018. [Online]. Available: https://cherab.github.io/documentation/index.html.

[9] M. Carr, A. Meakins, A. Baciero, M. Bernert, A. Callarelli, A. Field, C. Giroud, J. Harrison, N. Hawkes, S. Henderson, B. Lipschultz, Towards integrated data analysis of divertor diagnostics with ray-tracing, in: 44th EPS Conference on Plasma Physics, 2017.
[10] M. Carr, A. Meakins, Private Communication, 2019.
[11] M. Moscheni, Modeling the radiative power load on the EU-DEMO PFCs during a mitigated plasma disruption, Politecnico di Milano, 29 April 2020. [Online]. Available: https://www.politesi.polimi.it/handle/10589/153030. [Accessed 2020].
[12] A. Meakins, M. Carr, raysect/source: Release 0.5.5, Zenodo, 2019.
[13] A. Meakins, M. Carr, Raysect's documentation, 2018. [Online]. Available: https://raysect.github.io/documentation/index.html.
[14] F. Maviglia, C. Bachmann, G. Federici, T. Franke, M. Siccinio, C. Vorpahl, R. Albanese, R. Ambrosino, E. Fable, M. Firdaouss, J. Gerardin, V.P. Loschiavo, M. Mattei, F. Palermo, M.L. Richiusa, F. Villone, Z. Vizvary, Impact of plasma thermal transients on the design of the EU DEMO first wall protection, Fusion Eng. Des. 158 (2020) 111713.
[15] R.J. Moffat, Describing the uncertainties in experimental results, Exp. Therm Fluid Sci. 1 (1) (1988) 3–17.
[16] G. Pautasso, E. Fable, F. Koechl, P. Lang, M. Siccinio, F. Maviglia, Modelling of shattered pellet ablation: a discussion, in: 46th EPS Conference on Plasma Physics, vol. 3.1, 2019, pp. 3–6.
[17] S. Putvinski, Disruption mitigation in ITER, in: Proc. of 23rd IAEA Fusion Energy Conference, vol. 100, pp. ITR/1-6, 2010.
[18] F.C. Schuller, Disruptions in tokamaks, Plasma Phys. Controlled Fusion 37 (11A) (1995) A135–A162.
[19] J. Spanier, E.M. Gelbard, Monte Carlo Principles and Neutron Transport Problems, Dover Books of Mathematics, 2008.
[20] J. Linke, J. Du, T. Loewenhoff, G. Pintsuk, B. Spilker, I. Steudel, M. Wirtz, Challenges for plasma-facing components in nuclear fusion, Matter Radiat. Extremes 4(11) (5 2019) 056201.
[21] A. Huber, G. Arnoux, M.N.A. Beurskens, S.A. Bozhenkov, S. Brezinsek, T. Eich, C. Fuchs, W. Fundamenski, S. Jachmich, U. Kruezi, M. Lehnen, A. Loarte, G. F. Matthews, P. Mertens, P.D. Morgan, V. Philipps, R.A. Pitts, V. Riccardo, U. Samm, B. Schweer, G. Sergienko, M. Stamp, JET EFDA Contributors, Radiation loads onto plasma-facing components of JET during transient events – experimental results and implications for ITER, J. Nucl. Mater. 415 (1) (2011) S821–S827.